Biomedical Microdevices (2020) 22:36
https://doi.org/10.1007/s10544-020-00492-6

# Simultaneous electrical detection of IL-6 and PCT using a microfluidic biochip platform

Jacob Berger[1,2,3] · Enrique Valera[1,2,3] · Aaron Jankelow[1,2,3] · Carlos Garcia[1,2,3] · Manik Akhand[1,2] · John Heredia[1,2] · Tanmay Ghonge[1,2,3,4] · Cynthia Liu[1,2] · Victor Font-Bartumeus[1,2] · Gina Oshana[1,2] · Justin Tiao[1,2] · Rashid Bashir[1,2,3,5]



## Abstract

Sepsis, a life-threatening organ dysfunction caused by a dysregulated host response, leads the U.S in both mortality rate and cost of treatment. Sepsis treatment protocols currently rely on broad and non-specific parameters like heart and respiration rate, and temperature; however, studies show that biomarkers Interlukin-6 (IL-6) and Procalcitonin (PCT) correlate to sepsis progression and response to treatment. Prior work also suggests that using multi-parameter predictive analytics with biomarkers and clinical information can inform treatment to improve outcome. A point-of-care (POC) platform that provides information for multiple biomarkers can aid in the diagnosis and prognosis of potentially septic patients. Using impedance cytometry, microbead immunoassays, and biotin-streptavidin binding, we report a microfluidic POC system that correlates microbead capture to IL-6 and PCT concentrations. A multiplexed microbead immunoassay is developed and validated for simultaneous detection of both IL-6 and PCT from human plasma samples. Using the POC platform, we quantified plasma samples containing healthy, medium (~$10^3$pg/ml) and high (~$10^5$pg/ml) IL-6 and PCT concentrations with various levels of significance ($P < 0.05$-$P < 0.00001$) and validated the concept of this device as a POC platform for sepsis biomarkers.

**Keywords** Microfluidic electrical impedance · Protein detection · Micro-bead assay · IL-6 and PCT · Point-of-care diagnostics · Sepsis

## 1 Introduction

In 2016, an international panel of experts updated the third definition of sepsis and septic shock. Sepsis-3 is currently defined as life-threatening organ dysfunction caused by a dysregulated host response to infection (Singer et al. 2016). It is estimated that 31.5 million people develop sepsis each year, of which 19.4 million people progress to septic shock leading to 5.3 million deaths (Fleischmann et al. 2016). In the United States alone, sepsis is the leading cause of mortality and most expensive condition, with ~3.1 million cases per year with mortality rates of 20–50%, while also costing the U.S healthcare system $24 billion annually (Reddy et al. 2018).

The current protocol for screening potentially septic patients is the systemic inflammatory response syndrome (SIRS) criteria; heart and respiration rate, temperature (min/max), and white blood cell (WBC) count. Hospitals and intensive care units (ICU) have slight variations of when sepsis treatment protocol is implemented based on these criteria and their deviation from normal. Positive cases trigger the first step in identifying the source infection (Villegas and Moore 2018). Identifying bacterial infection requires up to 5 days of culture to attain a negative result, which is longer than the disease progression itself (Umlauf et al. 2013). This nonspecific tool, coupled with the inherently heterogeneous early

✉ Rashid Bashir
rbashir@illinois.edu

Tanmay Ghonge
tghonge@illumina.com

1 Department of Bioengineering, University of Illinois at Urbana-Champaign, 1102 Everitt Lab, MC 278, 1406 W. Green St, Urbana, IL 61801, USA

2 Holonyak Micro and Nanotechnology Lab, University of Illinois at Urbana-Champaign, 208 N. Wright St., Urbana, IL 61801, USA

3 Biomedical Research Center, Carle Foundation Hospital, 509 W University Ave., Urbana, IL 61801, USA

4 Present address: Illumina, San Diego, CA, USA

5 Carle Illinois College of Medicine, 807 South Wright St., Urbana, IL 61801, USA

Published online: 18 May 2020

onset symptoms of sepsis, is a major contributor to the difficulties in identification, diagnostics and management of this deadly disease. Several studies indicate that increased patient outcome occurs from rapid treatment to early sepsis identification (Seymour et al. 2017). One study showed that every delayed hour of antibiotic treatment can decrease 72 h survival rates by ~7.6% (Kumar et al. 2006). However, another study showed that early treatment of antibiotics did not increase survival rate compared to the controlled cohort (Alam et al. 2018). These studies highlight the difficulties and heterogeneity of this disease, and the requirements for personalized treatment.

Studies have demonstrated cell surface and proteome markers as viable biomarkers for sepsis stratification (Faix 2013). Engineering point-of-care (POC) platforms could be important to quantify various biomarkers as a fingerprint of the immune system for early stage sepsis. These could also be important to eventually allow patients to test these biomarkers before coming to emergency rooms and hospitals, and the test these markers in the hospitals rapidly and also over the patient stay to allow for rapid stratification of the patient and the disease (Reddy et al. 2018). The different stages of sepsis, pro-inflammatory and anti-inflammatory, have distinct biological signatures and result in different treatment requirement, which can be addressed by providing rapid and accurate biomarker information (Cohen et al. 2015; Liesenfeld et al. 2014).

Early stage pathological signals for sepsis include a hyper inflammatory immune response, and some potential biomarkers of interest have been correlated the hyperinflammatory, immunosuppressive and organ dysfunction phases of sepsis, including Interluken-6 (IL-6) and procalcitonin (PCT). IL-6 in particular has received increased attention as a promising biomarker for early identification of sepsis, with reported concentrations reaching >3000 pg/ml for ICU patients, while IL-6 levels in healthy adults are approximately 6.4 pg/ml (Faix 2013; Fernandez-Real et al. 2001). A meta-analysis by Hou et al on 6 studies concluded that IL-6 had a sensitivity of 85%, specificity of 62%, and was an accurate biomarker for sepsis identification (Hou et al. 2015). In addition to IL-6, several studies have mentioned PCT as a viable biomarker for sepsis (Standage and Wong 2011). Healthy PCT serum levels are approximately 12.7 pg/ml (Morgenthaler et al. 2002). Elevated PCT levels correlating to sepsis and sepsis shock range from 1 ng/ml- > 10 ng/ml, and returns to normal range in response to appropriate treatment faster than CRP, another potential biomarker for sepsis (Vijayan et al. 2017). A 2013 study of 177 SERS positive patients (78 of whom exhibited sepsis) concluded that abnormal PCT and IL-6 levels can serve as diagnostic and prognostic markers for sepsis, respectively (Jekarl et al. 2013).

Beyond correlations between single biomarker levels and sepsis progression, studies suggest that using predictive analytics and machine learning algorithms on both available parameters like electronic medical record (EMR) data and multiple biomarkers not currently screened in the clinics can help stratify and provide doctors information for timely treatment and intervention (Gultepe et al. 2013; Henry et al. 2015; Taneja et al. 2017; Tsoukalas et al. 2015). A POC platform providing multiple biomarker measurements can potentially dive decisions to improve outcomes for sepsis patients.

Optical bead-based multiplex assays have been developed for quantifying immune biomarkers. However, tests Lumiex's xMAP require a Luminex reader or flow cytometer that can range from $30,000 over $100,000, cost several hundred dollars per kit, and require a laboratory facility capable of operating and processing the samples. Technologies using microfluidic impedance cytometry has focused on finding a low cost alternative to flow cytometry, including applications for lab-on-a-chip and POC diagnostics (Sun and Morgan 2010). Attempting to overcome the costly requirements for large instrumentation and label free optical detection, other research has reported the use differential impedance cytometry to measure proteins; however these methods are single target, and generate a qualitative measurement compared to negative controls (Rodriguez-Trujillo et al. 2014). Other label free electrochemical techniques that achieve ultra-sensitive detection (e.g, carbon nanotube technologies, bio-field effect Transistors, and nanowires) often do not have a clinically relevant working range, or do not rapidly detect biomarkers for clinical applications (Malhotra et al. 2010; Rajan et al. 2013; Vacic et al. 2011).

Previous reports have utilized some combination of bead based immunodetection and capture for protein quantification. Aytur et al. reported a microchip platform that correlates bead capture to antigen concentration using only a sensor array and electrical read out, but is limited to a single target (Aytur et al. 2006). Mok et al. reported the use of a differential impedance capture platform for the detection of IL-6. However, this method only quantifies a single target (Mok et al. 2014). A POC platform developed by Xianyu et al. performs multiplexed detection of IL-6 and PCT from a single serum sample, however the chemiluminescent readout requires specifically tuned complex chemistry precursors to amplify the output signal and achieve a large dynamic range (Xianyu et al. 2018).

Our previous work has focused on POC devices for biomarker identification. The developed immunocapture biochip platform uses microfluidics, coulter counting, and biofunctionalization for target capture. This platform has demonstrated its potential for biomarker detection by successfully quantifying CD4/CD8 T cells for HIV/AIDS, demonstrated specific leukocyte counting from a drop of blood, and quantified nCD64 expression on neutrophils for sepsis stratification (Hassan et al. 2016, 2017; Watkins et al. 2013). Broadly, a cell or bead population is enumerated at an entrance counter with impedance cytometry. After entrance counting, the population of interest is specifically captured in a biofunctionalized

capture chamber containing a high surface area pillar array. Finally, impedance cytometry electrodes enumerate the remaining population. The differential measurement between the entrance and exit is used to calculate the target capture percentage. The quantification of your target analyte can be extrapolated from standard calibration curves correlated to capture rate.

Our most recent application of the this technology has been the successful demonstration of IL-6 quantification using a latex microbead sandwich immunoassay (Valera et al. 2018). This manuscript builds on the previous single protein assay, towards multiplexed detection capabilities, with the following data providing a proof of concept demonstration for simultaneous protein measurements from a single sample (Fig. 1). To the best of our knowledge, this manuscript reports the first multiplexed measurements using a differential immunocapture biochip platform. From 10 μL of undiluted plasma, the proposed POC platform measures abnormal IL-6 and PCT concentrations in clinically relevant ranges for sepsis using this POC modality and promotes this technology as multi-target quantification platform for sepsis diagnosis and management.

## 2 Materials and methods

### 2.1 Immunocapture biochip platform

The proposed Immunocapture Biochip Platform (IBP) is composed of two electrode groups and a capture chamber. The PCT and IL-6 Immunoassay Sandwich Complexes (ISC) are flowed across the entrance electrodes, enumerating the total population, then through the streptavidin functionalized capture chamber, and again across the exit electrodes to enumerate the non-captured beads (Fig. 2a, b). The efficacy and accuracy of this microfluidic enumeration method has been validated previously (Hassan et al. 2016).

A Wheatstone bridge circuit across 10 kΩ resistors is used to measure the impedance pulse amplitudes $Z_{AB}$ and $Z_{BC}$, and send the resulting signal to a differential amplifier to record impedance pulses as the beads cross the electrodes (Fig. 2c). Coulter counting impedance pulses result from a momentary disruption from the baseline current flowing through the conducting medium between the two electrodes. The (non-conducting) bead flows between the electrode and removes the conducting buffer and produces the measured impedance change. A small 15x30μm aperture is used to focus the bead flow across the aperture and to maximize the impedance pulse amplitude by creating the highest disruption in the buffer baseline current (Fig. 2d). Figure 2e shows a detailed view of the chamber geometry, with both 7 μm IL-6 beads and 9 μm PCT beads captured at 45°, the highest probability capture angel using this geometry. A detailed discussion of capture angle, analysis of shear stress, and effects of flow rate on target capture is previously described (Ghonge et al. 2017).

### 2.2 Fabrication

**Differential electrical counter** The molds used for the microfluidic aperture channels across the electrodes, as well as the pillared capture chamber were created using traditional

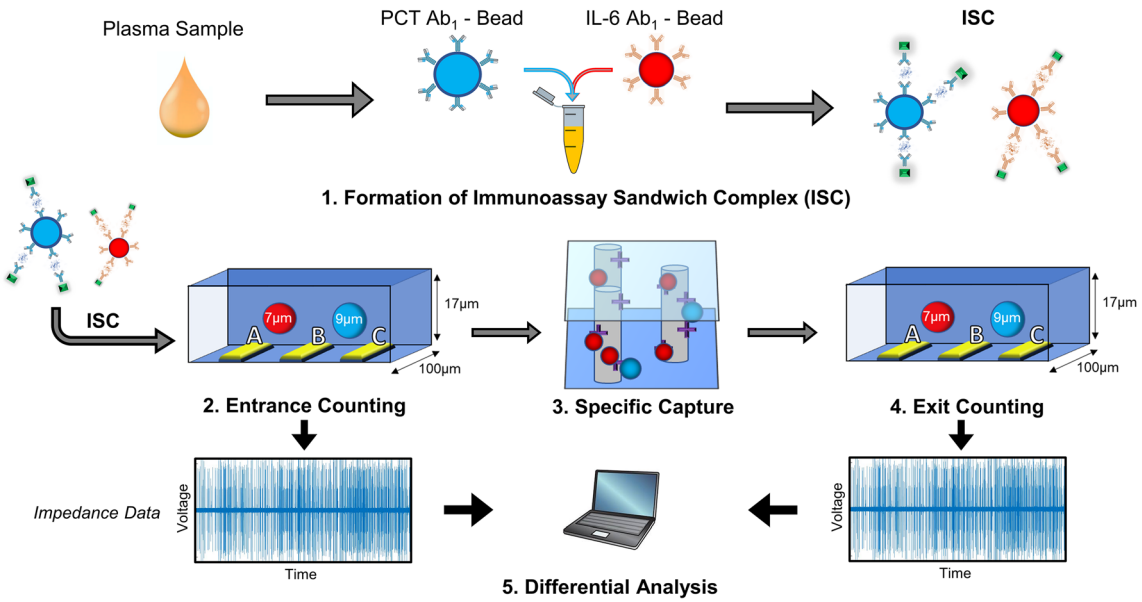


**Fig. 1** Outline for the multiplexed detection of PCT and IL-6 using electrical differential counting: 1) 10ul of plasma is incubated with microbeads to form an Immunoassay Sandwich Complex for PCT and IL-6 on the beads surface. 2) An entrance counter enumerates the ISC for PCT and IL-6 3) A portion of the beads are specifically captured based on the expression of PCT or IL-6 in the plasma sample. 4) An exit counter enumerates the exit population. 5) Differential analysis of the impedance data from the entrance and exit quantifies the expression range of PCT and IL-6 from plasma

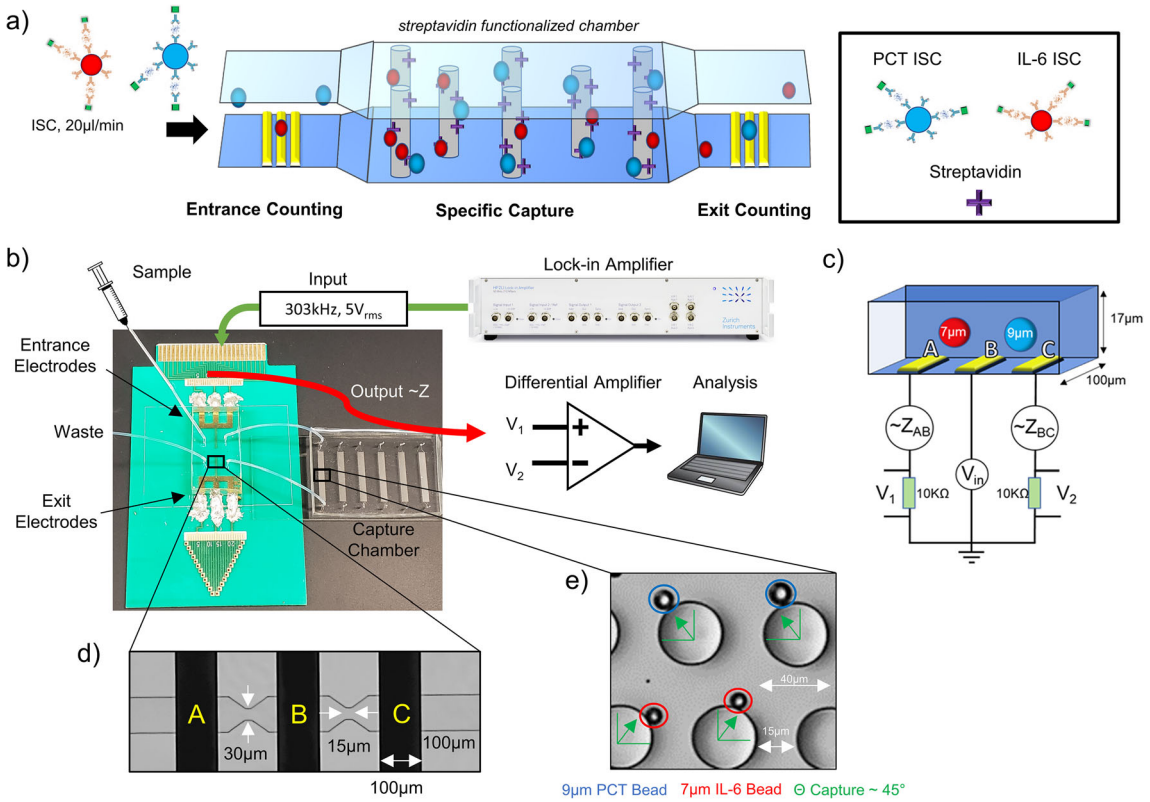


**Fig. 2** Overview of the Immunocapture Biochip Platform. (**a**) Experimental diagram of on chip dual capture. (**b**) Microfluidic differential electrical counter platform. Sample is flown over the set of entrance electrodes with an applied signal of 303 kHz, $5V_{rms}$ from the lock-in amplifier. Changes in impedance are generated from beads flowing over electrodes. Beads are captured specifically in a streptavidin functionalized chamber and enumerated over an exit counter, and a differential measurement is performed on the impedance data. (**c**) Wheatstone bridge circuit diagram of acquiring bipolar pulse impedance signals from 9 µm and 7 µm beads using 10 kΩ resistors. (**d**) Detailed image of aperture dimensions between counting electrodes used to maximize impedance pulses. **e** Image of 9 µm and 7 µm specific capture in streptavidin functionalized chamber pillars at the mean impact angle of 45° from dual capture experiments

lithography techniques using a 100 mm silicon wafer base (University Wafer) patterned with KMPR and SU-8 50 resists (MicroChem Corp) (Kim et al. 2008). The molds are used to make PDMS (Dow SYLGARD™ 184 Silicone Elastomer) channels using standard soft lithography techniques, which is described in detail elsewhere (Watkins et al. 2013).

The planar gold electrode array was fabricated on 4 in., 700 µm thick glass wafers (Schott borofloat 33 DSP) using traditional lift off lithographic techniques. The lithography procedure details of the impedance counters are described previously (Valera et al. 2018). To precisely place the apertures between the electrode arrays, the alignment time needed exceeds the rapid decay of surface activation using only $O_2$ plasma. To extend the surface activation time to allow for alignment, APTES/GPTMS chemistry protocol was used for bonding (Cortese et al. 2011; Tang and Lee 2010). The PDMS entrance and exit channel structure and the electrodes were activated with oxygen plasma, and placed into a 1% (*v*/v) solution of APTES and GPTMS respectively for 30 min at 60 °C. After the bath, the channels and electrodes were rinsed with DI water, dried with $N_2$ and aligned.

## 2.3 Functionalization

### 2.3.1 Capture chamber

The details of the chamber functionalization protocol have been described previously (Valera et al. 2018). Briefly, the capture chambers were first wetted with 70% ethanol to remove all the air bubbles, then flushed with PBS to remove the ethanol and prepare the device for streptavidin adsorption. A total of 35 µl of streptavidin solution (200 µg/ml) was flown through the capture chambers at 15 µl/min, then incubated for 30 min (repeated two times). After streptavidin adsorption, a total of 250ul of 1% BSA (*w*/*v*) was flown at 25 µl/min through the chambers and incubated for 60 min. All functionalization took place at room temperature. For all experimentation, all flow metering was done using a Harvard PHD ULTRA™ pump (Harvard Apparatus, MA, USA).

### 2.3.2 Microbead-antibody conjugation

Note, the previous assay used a latex microbead. Using magnetic instead of latex beads allows both the manipulation and

separation of the immunoassay building blocks on a microscale. The reported assay was optimized with magnetic instead of latex beads. (Jamshaid et al. 2016; Xiong et al. 2018; Yang et al. 2016). Two commercially available carboxyl active magnetic microbead populations (Absolute Mag™ Carboxyl Magnetic Particles, WHM-S035, WHM-S034, Creative Diagnostics) with mean diameters 9 μm and 7 μm were coupled with carbodiimide crosslinker chemistry to the primary PCT (cat#:abx019247, Abbexa) and IL-6 (cat#: M620, Thermofisher) capture $Ab_1$ respectively (Fig. 3a). Unless noted, both the PCT and IL-6 conjugation protocol steps are identical. All washing steps were performed on a magnetic separation rack (MagnaRack™, Invitrogen). 9 μm bead stock (50 μl, ~ $2.3 \times 10^6$ beads, 0.625 mg) and of 7 μm bead stock (25 μl ~$9.2 \times 10^5$ beads, 0.5 mg) were resuspended (5 s) and sonicated (ice bath, 3 s) in 400 μl MES buffer (0.1 M 2-(Nmorpholino)ethansulfonic acid, pH 6), and washed. This was repeated two more times with 500 μl of MES. Once the beads were washed 3x with MES, they were resuspended in a 200 μl EDC/NHS solution (1 mM EDC, 0.5 mM NHS respectively) then placed on a rotator (750 rpm, 20 min) in order to activate the carboxyl groups. After EDC/NHS activation, the beads were washed, and excess coupling reagents removed. Post surface activation, the 9 μm and 7 μm beads were functionalized in a PBS solution of $Ab_1$ PCT (200 μl, 200 μg/ml) and $Ab_1$ IL-6 (180 μl of 230 μg/ml) respectively, then placed on a rotator (750 rpm, 3 h). After surface functionalization, the beads were washed, and the supernatant collected for analysis. The beads were incubated with a blocking solution (0.1%BSA (*w*/*v*), 7.5 μg/ml glycine, 750rpm, 2 h). After blocking, the beads were washed 3x and stored in blocking solution (BlockAid™, Thermofisher) at 4 °C and were stable for about 8 weeks. The final concentration was ~27,000 beads/μl and 22,000 beads/μl for PCT and IL-6 respectively. The $Ab_1$ collected supernatant was quantified by a Bradford test (Bradford 1976), and estimated the efficiency of the conjugation was 82 ± 4% and 78 ± 5% for PCT and IL-6 respectively.

## 2.4 Formation of the immunoassay Sandwich complex

The final Immunoassay Sandwich Complex (ISC) consists of three components; the protein specific microbead (PCT-9 μm, IL-6-7 μm), the target protein, and the biotinylated secondary antibody ($Ab_2$-biotin). 10 μl of spiked plasma is added to a 90 μl of $Ab_1$ solution consisting of ~3375 ± 550 9 μm PCT and ~ 3142 ± 196 7 μm IL-6 Beads. The sample is placed on a rotator for 2 h at ~850 rpm for $Ab_1$ specific target capture. After specifically capturing the protein on the bead surface, the beads are washed two times to remove unbound target. The beads are resuspended in a 100 μl solution consisting of 8 μg/ml PCT $Ab_2$-biotin and 5 μg/ml IL-6 $Ab_2$-biotin and incubated at ~850 rpm for 30 min. After $Ab_2$-biotin incubation, the ISC is washed twice to remove excess $Ab_2$-biotin and is ready for testing on the differential immunocapture biochip (Fig. 3b).

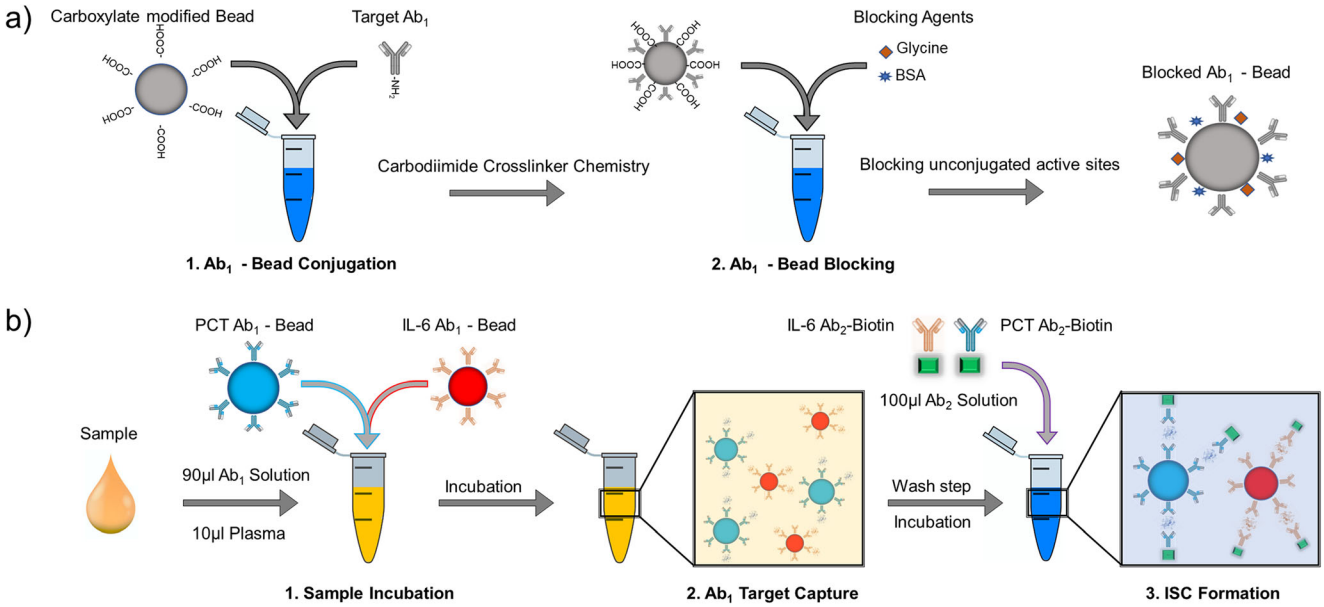


**Fig. 3** $Ab_1$ functionalization of the microbeads and construction of the ISC: (**a**) 1. Caboxylate beads are conjugated to the primary target $Ab_1$ using carbodiimide Crosslinker Chemistry. 2. Glycine and BSA block unconjugated active sights on $Ab_1$-beads to reduce non-specific binding. (**b**) 1. 10 μL of plasma is mixed with 90 μL of PCT/IL-6 $Ab_1$ Bead solution. 2. Incubation of plasma samples and $Ab_1$ beads leads to specific capture of IL-6 and PCT. A washing step is followed by incubation of a 100 μL PCT/IL-6 $Ab_2$ solution, which completes the formation of the ISC

### 2.5 Specificity and sensitivity validation of simultaneous targets

The functionality and compatibility of the ISC for each target was tested systematically by flow cytometry (Guava easyCyte, EMD Millipore) before measuring on the biochip. The ISC complex terminates in a biotin molecule, so following the ISC formation described in section 2.4, the beads were incubated with streptavidin-phycoerythrin (SAPE, ThermoFisher) (150 μl, 6.6 μg/ml, 30 min). The beads were washed twice to remove excess SAPE, resuspended in PBS and median florescence was measured. Forward scatter plots were used to distinguish the emissions from 9 μm-PCT and 7 μm-IL-6 populations in a single sample.

### 2.6 On-chip electrical differential measurements

#### 2.6.1 Raw data acquisition

The experimental measurement system for on-chip acquisition of the microfluidic differential counter data system is described in detail previously (Valera et al. 2018). In summary, after the formation of the ISC for PCT and IL-6 from a single spiked plasma sample (section 2.4), the ISC was resuspended in 150 μl PBS, loaded in a syringe, and flown over the entrance electrodes for an entrance count, into the streptavidin functionalized capture chamber, and finally over the exit electrodes for an exit count. The sigmoidal bipolar impedance pulses for the entrance and exit counts were generated by applying a 303 kHz, $5V_{rms}$ signal (HF2LI Lock-in amplifier, HF2CA Current amplifier, Zurich Instruments, Switzerland) to the middle electrode B, and measuring impedance pulse amplitudes $Z_{AB}$ and $Z_{BC}$ as a bead moves through the aperture between electrodes A-B and B-C. The output ~Z is sent to a differential amplifier and recorded on a customized LabVIEW (National Instruments, USA) code.

#### 2.6.2 Data processing

The raw data was sampled at 250kz and processed in a customized MATLAB (MathWorks, USA) code. The raw signal was filtered with digital post processing using native MATLAB functions; a 20 Hz high pass filter, 60 Hz and 120 Hz band stop filters for power line interference, and a low pass input frequency filter of 303 kHz. After filtering the data, histogram Analysis was done to enumerate and distinguish each bead population in both the entrance and exit counts. A histogram of peak voltage amplitudes was generated, and the two local minima were chosen to count the beads. Counts above the local minima between the noise and the first bead population distribution (7 μm IL-6 beads) gave the sum of beads enumerated at the counter. The second local minima distinguished between the 7 μm bead population distribution and the 9 μm bead population distribution.

The figure of merit for our differential counter is percent of target captured, expressed by a capture percentage of the target population that correlates with expression level. This is quantified as the differential measurement of the entrance and exit counts after capture within the chamber. Simply, it is the percent of beads captured in the chamber from the initial population.

## 3 Results and discussion

### 3.1 Validation of simultaneous capture

Before translating the developed microbead immunoassays onto our biochip platform, flow cytometry was used as a reference method to validate the experimental conditions of both the PCT and IL-6 sandwich immunoassay. SAPE was conjugated to the biotinylated end of the ISC, as described in section 2.5 (Fig. 4a), and the median SAPE fluorescence was recorded under various conditions ($n = 3$). The beads were tested across spiked samples with a concentration range of 0–$10^5$ pg/ml. First, the PCT and IL-6 beads were tested in isolation using target specific spiked samples to validate each individual ISC (Fig. 4b). These results suggested that the LOD for the PCT and IL-6 ISC was 130 pg/ml and 150 pg/ml respectively. Following the validation of each individual ISC, a systematic examination was performed on each ISC component to ensure both PCT and IL-6 can be captured and quantified simultaneously from a single sample.

PCT Immunoassays were then performed across three concentrations of IL-6 protein samples, and vice versa (Fig. 4c). Minimal fluorescence indicates low non-specific binding of $Ab_1$-beads to high concentrations of the off-target protein. To test the non-specific activity of the biotinylated secondary antibody, individual $Ab_1$ beads were conjugated across a range of target specific spiked samples, and then conjugated in a solution containing both biotinylated secondary antibodies (Fig. 4d, diagrams show components in each target specific reaction). both the PCT and IL-6 ISC maintained specificity in the presence of the off target nonspecific $Ab_2$.

After each individual ISC demonstrated sensitivity in the presence of both off target proteins and off-target secondary antibodies, calibration curves were constructed across a concentration range of 0–$10^5$ pg/ml for the PCT and IL-6 ISC, containing both high concentrations off the off target, as well as both target secondary antibodies (Fig. $4e_{1,2}$ inset diagram shows reaction components). After each ISC was able to capture and create a calibration curve across a range of target

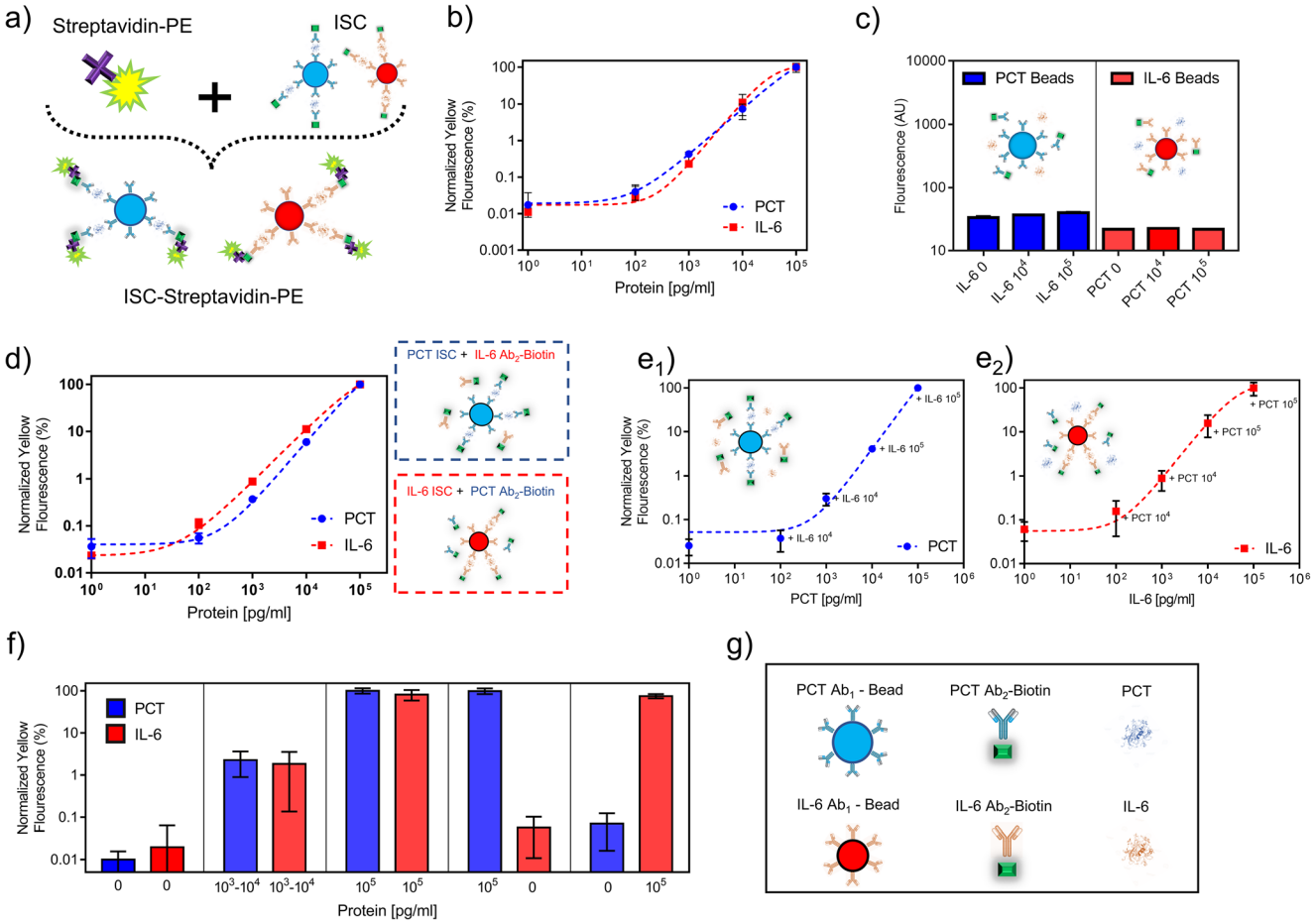


**Fig. 4** Validation and of Simultaneous Capture of PCT and IL-6. (**a**) Depiction of ISC conjugating to Streptavidin-PE for flow cytometry analysis. (**b**) Isolated LOD curves for PCT and IL-6 in spiked buffer to validate bead-$Ab_1$-protein capture ($n = 3$). (**c**) Testing each bead-$Ab_1$ with off target to confirm specificity. Inset diagram shows reaction components ($n = 3$). (**d**) Testing effects of off target $Ab_2$. Diagrams show assay components for PCT LOD curve and IL-6 LOD Curve ($n = 3$). (**e**) Isolated LOD Curves for PCT ($e_1$) and IL-6 ($e_2$) containing high off target concentrations and off target $Ab_2$ to demonstrate specificity and sensitivity of PCT and IL-6 sandwich assay. Inset diagram shows reaction components ($n = 3$). (**f**) Simultaneous capture of PCT and IL-6 from spiked plasma across 3 target concentrations, including high single target measurements. Each Plasma sample is incubated with both $Ab_1$ beads, and each bar graph pair indicates the signal from the PCT and IL-6 beads of that measurement ($n = 4$). (**g**) Legend

concentrations, in the presence of all off target ISC components, simultaneous dual capture experiments were performed.

The histogram in Fig. 4f is grouped by a PCT and IL-6 concentration in a single sample, and the corresponding signal intensity from PCT and IL-6 beads resulting from simultaneous target capture in the sample ($n = 4$). The developed immunoassay showed the ability to distinguish low, medium and high concentration samples of both targets, as well distinguishing between high/low concentration conditions for both PCT and IL-6. The validation procedure using flow cytometry confirms that a varying mean surface expression of conjugated ISC terminated with $Ab_2$-biotin on each bead surface is achieved using the established assay. The change of capture rate based on surface expression of the target has been demonstrated on both cells and beads in the differential biochip platform (Ghonge et al. 2017; Hassan et al. 2017).

## 3.2 On Chip electrical quantification

Using a 303 kHz interrogation frequency, the beads behave as insulators and generate impedance pulses proportional to bead size, and microbeads with different diameters generate unique signals for enumerating multiple populations across a single set of coulter electrodes. Distinguishable, size-dependent impedance pulses for 7 μm and 9 μm beads used for the development of the ISC were acquired (Fig. 5a) with the experimental set up.

The PDMS capture chamber (1.8 mm × 7.8 mm × 60 μm) was modified from a previous design for cell capture in order to capture beads. A specifically designed pillar geometry inside the chamber was used to maximize the functionalized surface area and bead capture probability. The pillar array dimensions in the capture chamber, 0.33/row stagger ratio, 40 μm pillar diameter, 15 μm spacing, were developed using

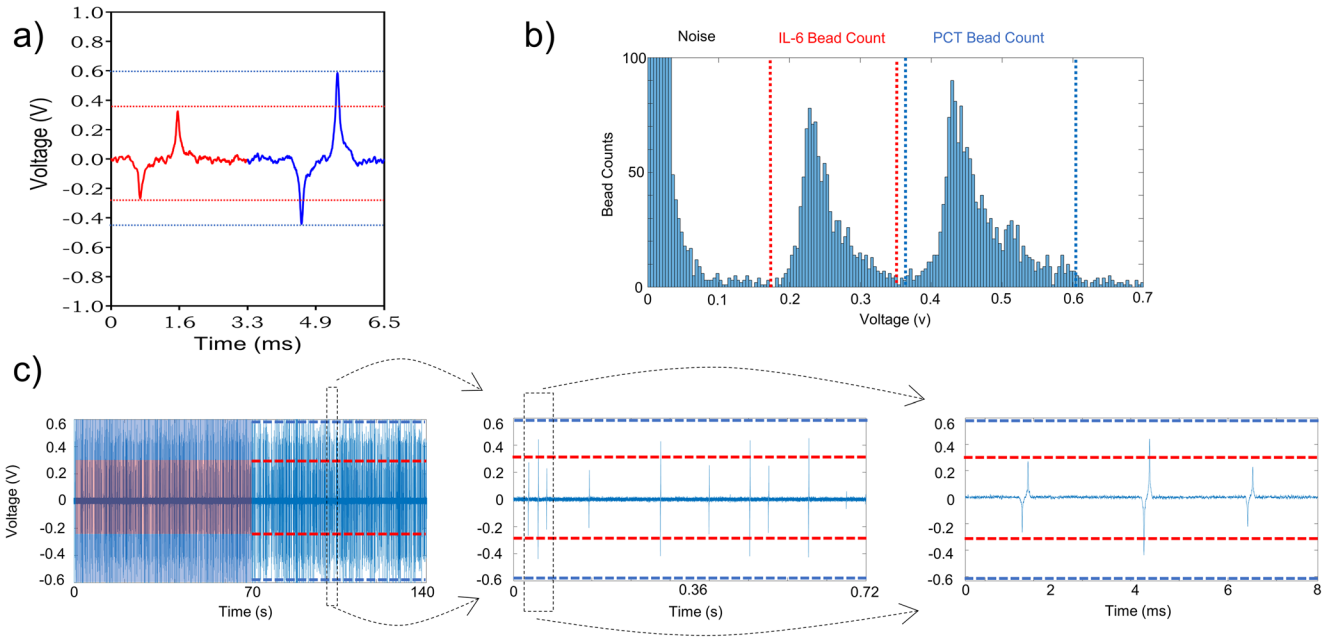


**Fig. 5** On Chip electrical Quantification. (**a**) Bipolar impedance pulse signals from 9 μm and 7 μm beads traveling across the differential electrical counter electrodes. Peak amplitudes are clearly distinguishable between beads. Entrance and exit counting generate both histograms and impedance data from the entrance and exit counters. (**b**) Generated histogram from on chip impedance measurements which can distinguishing noise, 7 μm and 9 μm bead signals. (**c**) Post-filtered impedance measurement generated from on chip detection, a visual validation of 7 μm and 9 μm bead signals that are binned in voltage histograms

a model by Inglis et al. to prevent clogging and create a linear particle flow path (Inglis et al. 2006).

After flowing the conjugated beads through the entrance counter, specifically capturing the biotinylated PCT/IL-6 ISC in the streptavidin functionalized capture chamber and enumerating the non-captured beads at the exit counter, the entrance and exit counting raw impedance data was processed. The entrance and exit histograms (Fig. 5b) enumerated the populations and solved for the percentage of capture (2.6.2). Across on chip dual capture experiments, the first local minima was 0.1 ± 0.033 V, and the second local minima was 0.27 ± 0.061 V. The average amplitude of the baseline noise was ~0.02 V, and the median pulse amplitudes were ~ 10X for the 7 μm IL-6 beads and ~ 22X for the 9 μm PCT beads compared to the baseline noise, allowing to clearly distinguish each bead population using the pulse amplitude distributions. After filtering, Fig. 5c shows a 140 s section of an impedance measurement, highlighting the bipolar pulse regions of the PCT and IL-6 beads with a blue and red band respectively. The dashed lines indicate the mean impedance pulse voltages, matching the amplitude obtained in a histogram, down to single pulses across an 8 ms time frame.

### 3.3 Simultaneous detection of IL-6 and PCT from plasma on chip

To validate the electrical differential counter for the simultaneous detection of PCT and IL-6, measurements were performed on controls, medium, and high concentrations in spiked plasma, using clinically relevant ranges for PCT and IL-6 expression. In addition, samples of expressing only high concentrations of either PCT or IL-6 were evaluated. For dual capture experiments, the ISC protocol was tested on a 10 μL plasma sample. The sample was flown at 20 μL/min through the entrance counter, streptavidin functionalized chamber, and exit counter, and the data acquisition recorded 100 μl of the resuspended sample for 5 min. An overlaid entrance and exit histogram for each condition are shown in Fig. 6a–e, which were used to calculate the percentage of capture. The x-axis voltage was normalized to visually align impedance measurements. Figure 6f shows a grouped box plot of each measurement condition ($n = 3$), with the respective protein concentration in that sample and the corresponding capture percentage of the 9 μm-PCT and 7 μm-IL-6 beads.

For both PCT and IL-6, the microfluidic biochip was able to distinguish with significance between healthy and high expression plasma samples, including samples with high off-target concentrations. For both PCT and IL-6, our biochip platform was able to distinguish with significance medium range expression vs high expression, including plasma samples with high a concentration off-target. No statistical significance was attained between controls and medium concentrations, due to the large standard deviation in the medium control experiments, however the mean capture expression suggests a clear trend between healthy, medium expression and high expression samples for both PCT and IL-6. One

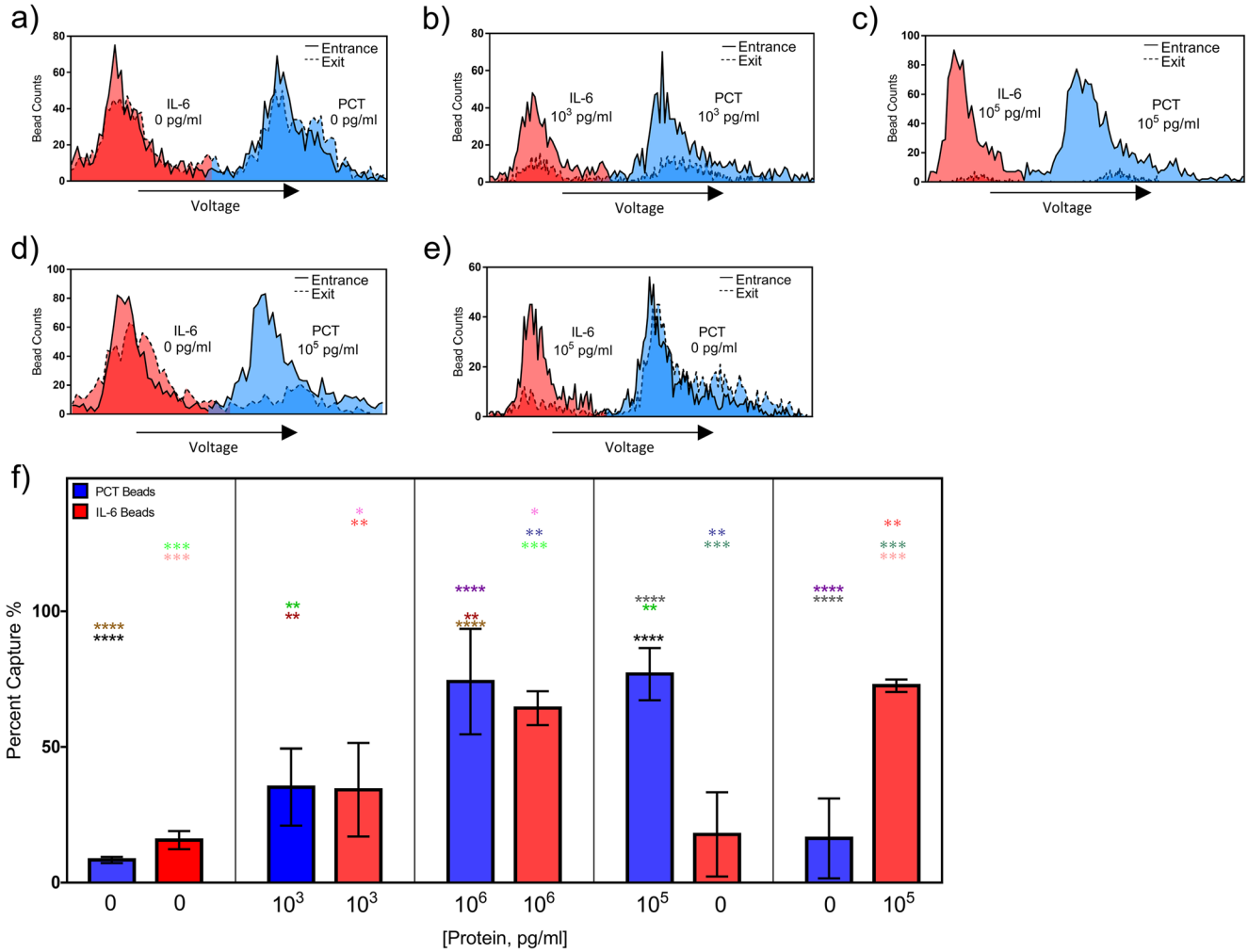


**Fig. 6** Simultaneous detection of IL-6 and PCT from plasma on chip. (**a**–**e**) Overlaid entrance and exit histograms for on-chip dual capture measurement conditions: red area is IL-6 bead signal, and blue area is PCT bead signal. (**f**) Histogram of on chip dual capture conditions: percent captured per condition for both PCT and IL-6 beads. Significance is measured between percent capture for each type bead comparing each condition ($n = 3$). (2way ANOVA, $\alpha = 0.05$, *: $p < 0.05$, **: $P < 0.001$, ***: $P < 0.0001$, ****: $P < 0.00001$)

explanation for these variations is the difference in final bead count for both populations. Control counts using flow cytometry showed the mean populations of ~3375 ± 550 9 μm PCT and ~ 3142 ± 196 7 μm IL-6 beads, a large inherent deviation even before all washing steps, along with bead loss from non-specific adsorption in all the microfluidic components. This variation may lead to changes in available binding sites throughout the capture chamber, leading to an increased standard deviation from the same sample conditions. Developments to improve non-specific capture rate, as well as consistency in bead population per assay can increase the quantification sensitivity of this platform.

If additional multiplexing of more markers will be integrated in this platform, this work also highlights the need to develop new types immunocapture microbeads, which are of the same size but should have a different electrical signature. Having beads of the same size and similar density would allow them to experience similar shear stress during the capture on the post-arrays with the device.

Translating immunoassay assembly to the microscale can save time and reagent cost, and further move towards addressing the technical needs at point of care. Future directions of this platform can integrate both immunoassay assembly and separation of proteome markers from whole blood samples. By combining this work with previously established cell-surface biomarker quantification, this work moves this platform towards a multiplexed quantification modality for both cells and proteins.

## 4 Conclusions

A microbead based platform for the simultaneous detection of PCT and IL-6 has been developed, and the assay performance

was tested on spiked undiluted human plasma samples. First, individual microbead sandwich immunoassays were developed for both PCT (LOD 130 pg/ml) and IL-6 (150 pg/ml), and the compatibility for multiplexed capture verified by flow cytometry. These immune sandwich complexes (ISC's), which simultaneously captured varying ranges of PCT and IL-6 from a single undiluted plasma sample, were flown through an established microfluidic biochip platform. This new application demonstrated the ability to differentiate with significance, varying expression conditions for both PCT and IL-6 in the clinically relevant range of potentially septic patients. Several improvements are necessary for both increases in quantification range and clinical application. However, as proof of principle, this manuscript highlights this multiplexed capture detection platform with promising applications to differentiate healthy from potentially septic patients with varying ranges of PCT and IL-6 concentrations.

**Acknowledgements** The authors thank A. Hasnain, V. Kindratenko, M. Saadah, and A. Bobat for their help on devices fabrication. The authors acknowledge the support of Center for Integration of Medicine and Innovative Technology Innovation (CIMIT)'s Point-of-Care Technology Center in Primary Care (POCTRN) Grant, the support of NIH (project number 1 R21 AI146865 A), and funding from University of Illinois at Urbana-Champaign.

**Author contributions** J.B, E.V, and R.B conceived of and designed the study. J.B wrote and E.V and R.B edited the manuscript. J.B, E.V, and A.J performed the experiments. J.B, E.V, and A.J worked on Matlab Code and Analyzed data. E.V and T.G designed the devices. C.G, M.A, J.H, C.L, V.F, G.O and J.T fabricated the devices and prepared experimental reagents.

## Compliance with ethical standards

**Conflict of interest** Rashid Bashir declares competing financial interests in Prenosis, Inc. working to commercialize technologies for detection of cells and proteins.

## References

N. Alam et al., Prehospital antibiotics in the ambulance for sepsis: a multicentre, open label, randomised trial. Lancet Respir. Med. **6**(1), 40–50 (2018)

T. Aytur et al., A novel magnetic bead bioassay platform using a microchip-based sensor for infectious disease diagnosis. J. Immunol. Methods **314**(1), 21–29 (2006)

M.M. Bradford, A rapid and sensitive method for the quantitation of microgram quantities of protein utilizing the principle of protein-dye binding. Anal. Biochem. **72**(1), 248–254 (1976)

J. Cohen et al., Sepsis: a roadmap for future research. Lancet Infect. Dis. **15**(5), 581–614 (2015)

B. Cortese, M.C. Mowlem, H. Morgan, Characterisation of an irreversible bonding process for COC-COC and COC-PDMS-COC sandwich structures and application to microvalves. Sensors Actuators B Chem. **160**(1), 1473–1480 (2011)

J.D. Faix, Critical reviews in clinical laboratory sciences biomarkers of Sepsis biomarkers of Sepsis*. Crit. Rev. Clin. Lab. Sci. **50**(501), 23–36 (2013)

J.M. Fernandez-Real et al., Circulating interleukin 6 levels, blood pressure, and insulin sensitivity in apparently healthy men and women. J. Clin. Endocrinol. Metab. **86**(3), 1154–1159 (2001)

C. Fleischmann et al., Assessment of global incidence and mortality of hospital-treated sepsis current estimates and limitations. Am. J. Respir. Crit. Care Med. **193**(3), 259–272 (2016)

T. Ghonge et al., A microfluidic technique to estimate antigen expression on particles. APL Bioeng. **1**(1), 016103 (2017)

E. Gultepe et al., From vital signs to clinical outcomes for patients with Sepsis: a machine learning basis for a clinical decision support system. J. Am. Med. Inform. Assoc. **21**(2), 315–325 (2013)

U. Hassan et al., Microfluidic differential Immunocapture biochip for specific leukocyte counting. Nat. Protoc. **11**(4), 714–726 (2016)

U. Hassan et al., A point-of-care microfluidic biochip for quantification of CD64 expression from whole blood for Sepsis stratification. Nat. Commun. **8**(1), 15949 (2017)

K.E. Henry, D.N. Hager, P.J. Pronovost, S. Saria, A targeted real-time early warning score (TREWScore) for septic shock. Sci. Transl. Med. **7**(299), LP 299ra122 (2015)

T. Hou et al., Accuracy of serum interleukin (IL)-6 in sepsis diagnosis: a systematic review and meta-analysis. Int. J. Clin. Exp. Med. **8**(9), 15238–15245 (2015)

D.W. Inglis, J.A. Davis, R.H. Austin, J.C. Sturm, Critical particle size for fractionation by deterministic lateral displacement. Lab Chip **6**(5), 655–658 (2006)

T. Jamshaid et al., Magnetic particles: from preparation to lab-on-a-Chip, biosensors, microsystems and microfluidics applications. TrAC Trends Anal. Chem. **79**, 344–362 (2016)

D.W. Jekarl et al., Procalcitonin as a diagnostic marker and IL-6 as a prognostic marker for sepsis. Diagn. Microbiol. Infect. Dis. **75**(4), 342–347 (2013)

P. Kim et al., Soft lithography for microfluidics: a review. Biochip J. **2**(1), 1–11 (2008)

A. Kumar et al., Duration of hypotension before initiation of effective antimicrobial therapy is the critical determinant of survival in human septic shock. Crit. Care Med. **34**(6), 1589–1596 (2006)

O. Liesenfeld, L. Lehman, K.-P. Hunfeld, G. Kost, Molecular diagnosis of sepsis: new aspects and recent developments. Eur. J. Microbiol. Immunol. **4**(1), 1–25 (2014)

R. Malhotra et al., Ultrasensitive electrochemical immunosensor for oral cancer biomarker IL-6 using carbon nanotube forest electrodes and multilabel amplification. Anal. Chem. **82**(8), 3118–3123 (2010)

J. Mok, M.N. Mindrinos, R.W. Davis, M. Javanmard, Digital microfluidic assay for protein detection. Proc. Natl. Acad. Sci. U.S.A. **111**(6), 2110 LP–2112115 (2014)

N.G. Morgenthaler et al., Detection of procalcitonin (PCT) in healthy controls and patients with local infection by a sensitive ILMA. Clin. Lab. **48**(5–6), 263–270 (2002)

N.K. Rajan, X. Duan, M.A. Reed, Performance limitations for nanowire/nanoribbon biosensors. Wiley Interdiscip. Rev. Nanomed. Nanobiotechnol. **5**(6), 629–645 (2013)

B. Reddy et al., Point-of-care sensors for the management of sepsis. Nat. Biomed. Eng. **2**(9), 640–648 (2018)

R. Rodriguez-Trujillo et al., Label-free protein detection using a microfluidic coulter-counter device. Sensors Actuators B Chem. **190**, 922–927 (2014)

C.W. Seymour et al., Time to treatment and mortality during mandated emergency care for sepsis. N. Engl. J. Med. **376**(23), 2235–2244 (2017)

M. Singer et al., The third international consensus definitions for sepsis and septic shock (Sepsis-3). JAMA **315**(8), 801 (2016)

S.W. Standage, H.R. Wong, Biomarkers for pediatric sepsis and septic shock. Expert Rev. Anti-Infect. Ther. **9**(1), 71–79 (2011)

T. Sun, H. Morgan, Single-cell microfluidic impedance cytometry: a review. Microfluid. Nanofluid. **8**(4), 423–443 (2010)

I. Taneja et al., Combining biomarkers with EMR data to identify patients in different phases of sepsis. Sci. Rep. **7**(1), 10800 (2017)

L. Tang, N.Y. Lee, A facile route for irreversible bonding of plastic-PDMS hybrid microdevices at room temperature. Lab Chip **10**(10), 1274–1280 (2010)

A. Tsoukalas, T. Albertson, I. Tagkopoulos, From data to optimal decision making: a data-driven, probabilistic machine learning approach to decision support for patients with Sepsis. JMIR Med. Inform. **3**(1), e11 (2015)

V.N. Umlauf, S. Dreschers, T.W. Orlikowsky, Flow cytometry in the detection of neonatal sepsis. Int. J. Pediatr. **2013**, 1–6 (2013)

A. Vacic et al., Multiplexed SOI BioFETs. Biosens. Bioelectron. **28**(1), 239–242 (2011)

E. Valera et al., A microfluidic biochip platform for electrical quantification of proteins. Lab Chip **18**(10), 1461–1470 (2018)

A.L. Vijayan et al., Procalcitonin: a promising diagnostic marker for sepsis and antibiotic therapy. J. Intensive Care **5**(1), 1–7 (2017)

N. Villegas, L.J. Moore, Sepsis screening: current evidence and available tools. Surg. Infect. **19**(2), 126–130 (2018)

N.N. Watkins et al., Microfluidic CD4+ and CD8+ T lymphocyte counters for point-of-care HIV diagnostics using whole blood. Sci. Transl. Med. **5**(214), (2013). https://doi.org/10.1126/scitranslmed.3006870

Y. Xianyu et al., Controllable assembly of enzymes for multiplexed lab-on-a-chip bioassays with a tunable detection range. Angew. Chem. Int. Ed. **57**(25), 7503–7507 (2018)

Q. Xiong et al., Magnetic nanochain integrated microfluidic biochips. Nat. Commun. **9**(1), 1–11 (2018)

R.-J. Yang, H.-H. Hou, Y.-N. Wang, F. Lung-Ming, Micro-magnetofluidics in microfluidic systems: a review. Sensors Actuators B Chem. **224**, 1–15 (2016)